

Creation and control of a two-dimensional electron liquid at the bare SrTiO₃ surface

W. Meevasana^{1,2,3,4,5†}, P. D. C. King^{3†}, R. H. He^{1,2,6}, S-K. Mo^{1,6}, M. Hashimoto^{1,6}, A. Tamai³, P. Songsiririthigul^{4,5}, F. Baumberger³ and Z-X. Shen^{1,2★}

Many-body interactions in transition-metal oxides give rise to a wide range of functional properties, such as high-temperature superconductivity¹, colossal magnetoresistance² or multiferroicity³. The seminal recent discovery of a two-dimensional electron gas (2DEG) at the interface of the insulating oxides LaAlO₃ and SrTiO₃ (ref. 4) represents an important milestone towards exploiting such properties in all-oxide devices⁵. This conducting interface shows a number of appealing properties, including a high electron mobility^{4,6}, superconductivity⁷ and large magnetoresistance⁸, and can be patterned on the few-nanometre length scale. However, the microscopic origin of the interface 2DEG is poorly understood. Here, we show that a similar 2DEG, with an electron density as large as $8 \times 10^{13} \text{ cm}^{-2}$, can be formed at the bare SrTiO₃ surface. Furthermore, we find that the 2DEG density can be controlled through exposure of the surface to intense ultraviolet light. Subsequent angle-resolved photoemission spectroscopy measurements reveal an unusual coexistence of a light quasiparticle mass and signatures of strong many-body interactions.

It has been known for decades that strong electron correlations in oxide materials give rise to a rich variety of electronic phases, which are highly susceptible to small changes of control parameters. Although this situation is ideal for applications, the potential of all-oxide electronic devices had been questioned until very recently. Indeed, it was thought that the chemical complexity of most oxides would yield devices much inferior to those based on conventional semiconductors⁵. A paradigm shift came when unprecedented control of the complex LaAlO₃/SrTiO₃ interface was demonstrated⁴, leading to the formation of a high-mobility electron gas⁶. The carrier density and sheet conductivity of the interface 2DEG react sensitively to gate fields and it was successfully patterned on the nanoscale⁹, which is central to the development of oxide electronics¹⁰. However, a full understanding of the origin of this 2DEG remains elusive. The two main contenders are oxygen vacancies at the interface^{11,12}, and an electronic reconstruction to avoid a polar catastrophe^{4,13}. Distinguishing between these mechanisms is an essential step in the development of a new generation of all-oxide devices.

Here, we show that a similar 2DEG can be created at the bare, unreconstructed SrTiO₃ surface. Furthermore, we demonstrate control of its carrier density through exposure to intense ultraviolet radiation. Figure 1 shows angle-resolved photoemission spectroscopy (ARPES) data from the cleaved (001) surface of

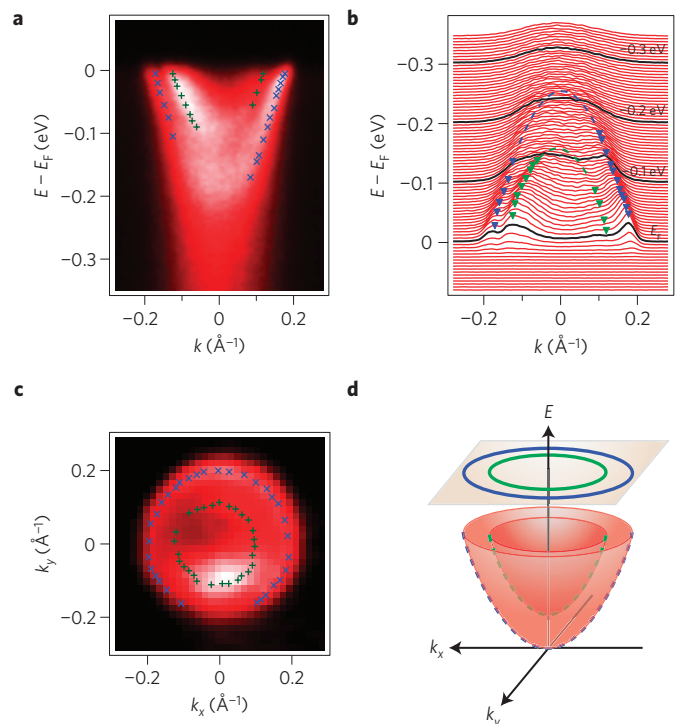


Figure 1 | Observation of a surface 2DEG on SrTiO₃ after exposure of the cleaved (100) surface to synchrotron (ultraviolet) light. **a, b**, ARPES data of La_xSr_{1-x}TiO₃ ($x = 0.001$) at $T = 20 \text{ K}$ (**a**), with corresponding momentum distribution curves (**b**). The sample has been irradiated with $\approx 480 \text{ J cm}^{-2}$ ultraviolet light of 55 eV with an intensity of $\sim 0.34 \text{ W cm}^{-2}$. The ARPES data are taken in the second Brillouin zone using the same photon energy. The dashed lines in **b** are parabolic fits to the data points (symbols) extracted from the ARPES data; the green and blue curves have effective masses of ~ 0.6 and $0.5m_e$, respectively. **c**, Fermi surface map, taken on a different sample following the same preparation. Two concentric circular Fermi surface sheets (symbols) are visible. **d**, The schematic Fermi surface and band dispersions obtained from the measured electronic structure.

0.1% La-doped SrTiO₃(001) following exposure to ultraviolet synchrotron light. At least two electron-like band dispersions can be observed from the ARPES data (Fig. 1a,b). The shallower band, with Fermi wave number $k_F = 0.12 \text{ \AA}^{-1}$, and deeper band,

¹Departments of Physics and Applied Physics, Stanford University, California 94305, USA, ²Stanford Institute for Materials and Energy Sciences, SLAC National Accelerator Laboratory, 2575 Sand Hill Road, Menlo Park, California 94025, USA, ³School of Physics and Astronomy, University of St. Andrews, North Haugh, St. Andrews, KY16 9SS, UK, ⁴School of Physics, Suranaree University of Technology and Synchrotron Light Research Institute, Nakhon Ratchasima, 30000, Thailand, ⁵Thailand Center of Excellence in Physics, CHE, Bangkok, 10400, Thailand, ⁶Advanced Light Source, Lawrence Berkeley National Lab, Berkeley, California 94720, USA. [†]These authors contributed equally to this work. *e-mail: zxshen@stanford.edu.

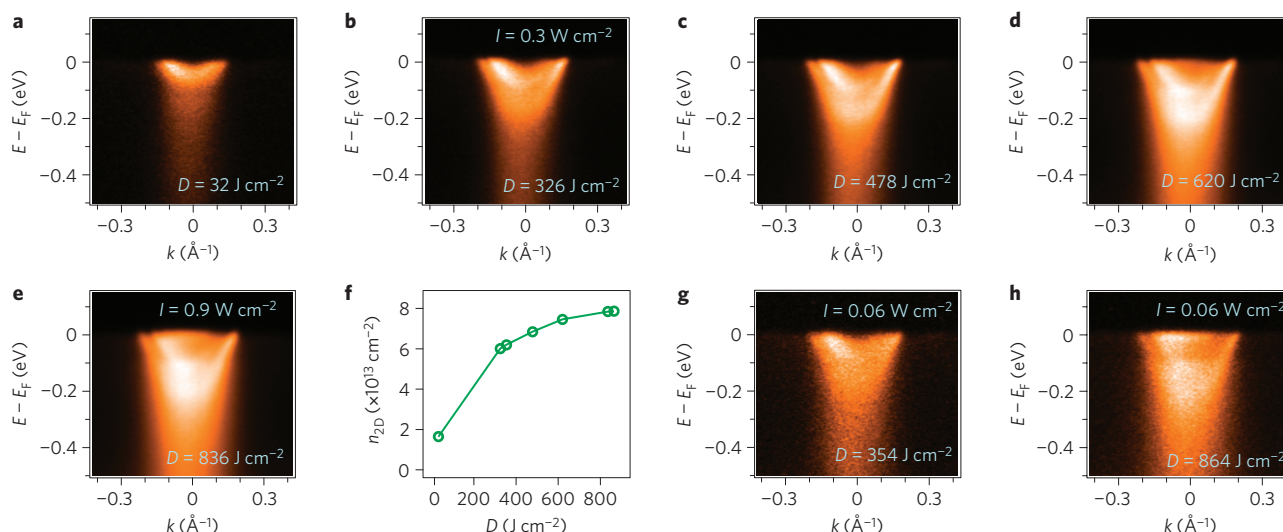


Figure 2 | Variation of 2DEG charge density with exposure to different ultraviolet irradiation doses. a–h, ARPES data for the specified irradiation doses (**a–e, g, h**), and the corresponding 2DEG charge densities as a function of irradiation dose, D (**f**). **g** and **h** show ARPES data measured immediately after **b** and **e**, respectively, but with a lower intensity of the probing photon beam.

with $k_F = 0.175 \text{ \AA}^{-1}$, have their band bottoms situated ~ 110 and 216 meV below the Fermi level, respectively. We have investigated the dimensionality of the induced electronic system by varying the photon energy, and thus probing the band dispersion along k_z (surface normal). Supplementary Fig. S2 shows that the states have negligible dispersion along k_z . This is the defining property of a two-dimensional (2D) electronic state whose wavefunction is confined along the z -direction to a layer of comparable thickness to the Fermi wavelength. In addition, these bands cannot be associated with the bulk electronic structure: the photon energy used to record the data shown in Fig. 1 corresponds to k_z of approximately $3.2\pi/a$ (ref. 14), close to the Brillouin zone boundary where no bulk bands exist in the vicinity of the Fermi energy, even for samples with more than an order of magnitude higher bulk carrier density than those measured here. Consequently, we attribute these states to a surface 2DEG.

To obtain the surface charge density, we extract the Luttinger area from the Fermi surface map shown in Fig. 1c. Two concentric Fermi surface sheets are observed, corresponding to the two dispersions in Fig. 1a. The intensity variation across the measured Fermi surface is due to pronounced matrix element effects. The charge density n_{2D} from each concentric sheet can then be estimated by $n_{2D} = k_F^2/2\pi$, allowing the total surface charge density to be determined as $7.1 \pm 2 \times 10^{13} \text{ cm}^{-2}$. This value falls within the range of the 2DEG densities observed at $\text{LaAlO}_3/\text{SrTiO}_3$ interfaces^{7,11,12}. The effective masses extracted from parabolic fits to the two measured dispersions (Fig. 1a) yield surprisingly low values of $0.5\text{--}0.6m_e$, substantially lower than the bulk band masses. This will contribute to the high electron mobility⁴.

Furthermore, as shown in Fig. 2, we find that the 2DEG density is not fixed to one particular value, but can be varied by exposure of the cleaved surface to different irradiation doses of ultraviolet light. We found no evidence of any 2DEG states from initial ARPES measurements of the freshly cleaved surface, indicating that the 2DEG forms only after exposure to ultraviolet light. Following exposure to 55 eV ultraviolet light for an irradiation dose of $\sim 32 \text{ J cm}^{-2}$ (Fig. 2a), we observe a single shallow band with $k_F \sim 0.1 \text{ \AA}^{-1}$ and a band bottom $\sim 60 \text{ meV}$ below E_F . On increasing the irradiation dose, this band moves downwards, to higher binding energies, with a second band becoming visible between the first band and the Fermi level. The k_F positions and occupied bandwidth of these two bands continue to increase slowly with further increases

in irradiation dose. The corresponding surface charge densities extracted from the measured bands are plotted in Fig. 2f, revealing a monotonic increase in 2DEG density with increasing irradiation dose. Therefore, the method used here provides a controllable means with which to modify the 2DEG density.

We note that Fig. 2g and h, which are measured immediately after Fig. 2b and e, respectively, but with a lower intensity of the probing beam ($I = 0.06 \text{ W cm}^{-2}$), show identical band dispersions within experimental accuracy. Similar results have been obtained for spectra taken up to an hour after irradiation with an intense ultraviolet beam (not shown). This demonstrates that the 2DEG reported here is a ground-state property of the ultraviolet-irradiated SrTiO_3 surface. Hence, its origin must be fundamentally different from photocarrier doping effects, which have characteristic lifetimes of the excited states $< 1 \text{ ms}$ at low temperature¹⁵.

It is clear, therefore, that the irradiation by ultraviolet light mediates a change in the surface of the SrTiO_3 , which consequently induces the 2DEG. Clear (1×1) low-energy electron diffraction patterns observed both before and after the ultraviolet exposure indicate that the surface does not reconstruct during this process (see Supplementary Fig. S1). Therefore, creation of a surface 2DEG brought about by a change in the intrinsic surface state distribution due to surface reconstruction can be ruled out. This indicates that extrinsic states, such as donor-like defects or adsorbates, induce the 2DEG. In particular, oxygen vacancies localized at the surface would be expected to lead to a surface electron accumulation, with charge neutrality requiring the creation of an electron 2DEG to screen the positive surface charge of such ionized defect centres. Experimental studies on $\text{LaAlO}_3/\text{SrTiO}_3$ interfaces^{11,12} have shown that oxygen vacancies can be created during the sample preparation process under low oxygen pressures. Here, we suggest that exposure to intense ultraviolet light in ultrahigh vacuum causes oxygen desorption from the surface. Such a photon-induced chemical change was previously observed in photoluminescence spectra of SrTiO_3 following irradiation with 325 nm laser light¹⁶, where a sub-bandgap luminescence peak, growing in magnitude with increasing irradiation, and stable for some time following the irradiation, was assigned to photo-induced oxygen vacancies. This is consistent with an increased in-gap defect state (ref. 17 and references therein) that we observe at $\sim 1.3 \text{ eV}$ below the Fermi level in angle-integrated photoemission spectra following the ultraviolet exposure (see Supplementary Information).

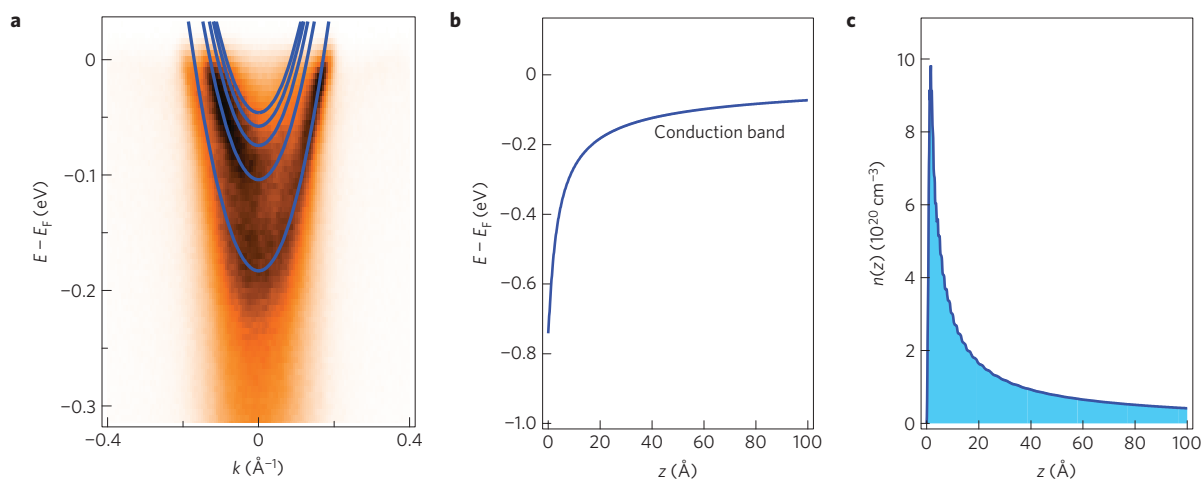


Figure 3 | Calculations of quantized 2DEG states within a band-bending model²⁰. **a, b**, The calculations yield quantized 2DEG states (solid lines in **a**) inside the potential well caused by the downward bending of the conduction band minimum (solid line in **b**) relative to the Fermi level, when approaching the surface of the material. **c**, The corresponding 3D charge density variation as a function of depth, z . We note that in the calculation, there are three additional shallow states that are not clearly observed in the data. It is possible that these states exist in the data but are suppressed owing to a combination of matrix element effects and broadening due to finite k_x dispersion of the shallow states. These considerations are supported by the observations from InAs (Fig. 4b), as well as other semiconductors^{24,28}, where shallow states of a surface quantum well are more smeared out than the deeper ones.

We cannot exclude that this in-gap state could also arise from adsorbed impurities such as hydrogen, which could themselves provide the required donor-type surface states, as discussed in the Supplementary Information. However, irrespective of the exact microscopic identification of the defects causing the charge accumulation, the results presented above demonstrate that it is not necessary to have an interface with the polar surface of another material to obtain a 2DEG at the surface of SrTiO₃. Indeed, we find that extrinsic mechanisms are sufficient to induce a ground-state 2DEG of the same density. Apart from obvious advantages for their spectroscopic investigation, the methodology employed here to create such a 2DEG offers potential for the realization of new schemes in oxide electronics. Although existing approaches have the ability to pattern the spatial extent of the LaAlO₃/SrTiO₃ interface 2DEG (refs 9,18), our work opens the way to spatial control of its ground-state density by employing focused light. Furthermore, ultraviolet interference patterns could be used to allow much faster parallel nanoscale patterning of the 2DEG. This should not be specific to the surface of SrTiO₃, and could be employed for creation of surface 2DEGs across a range of oxide materials. The scheme should also be useful to write surface charge on LaAlO₃ by desorbing oxygen. For a thin layer of LaAlO₃ grown on SrTiO₃, charge localized at the surface of the LaAlO₃ is thought to provide the mechanism for writing of metallic lines at the LaAlO₃/SrTiO₃ interface using conducting atomic-force microscopy¹⁹. Writing of surface charge on the LaAlO₃ layer using ultraviolet interference patterns could therefore be an attractive route towards efficient processing of a high-mobility modulation-doped 2DEG, patterned at the nanoscale.

To further characterize the 2DEG created here, we adapt a model originally developed for conventional semiconductors²⁰. The charge resulting from surface- (or indeed interface-) localized oxygen vacancies induces a spatial redistribution of bulk carriers in the vicinity of the surface/interface, correlated with a bending of the electronic bands relative to the Fermi level. If the potential well created by this band bending is sufficiently deep, it causes the conduction band states to become quantized into 2D sub-bands. We have carried out coupled Poisson–Schrödinger calculations²⁰ for such a band-bending scenario. Incorporating an electric-field dependence of the susceptibility²¹ within our model, we find that the downward

band bending in SrTiO₃ (Fig. 3b) is indeed very rapid. This leads to a narrow 2DEG (Fig. 3c) in a 3D crystal due only to the strength of the internal electric field. Its lowest sub-band is localized within ≈ 4 unit cells from the surface and is followed by a series of higher sub-bands with wavefunctions that progressively extend deeper into the bulk (see Supplementary Fig. S4). As shown in Fig. 3a, these sub-bands effectively reproduce the two main dispersions observed in the ARPES data, confirming that the states observed here can broadly be described as the quantum-well states of a surface 2DEG resulting from a downward band bending. The additional weakly bound states found in the calculations at lower binding energies are not resolved experimentally. This is possibly due to low matrix elements for shallow quantum-well states, which generally have small amplitudes of the wavefunction in the near-surface region probed by ARPES, as shown in Supplementary Fig. S4. Furthermore, as the wavefunctions of these shallow states expand over a much larger depth than the more localized deeper states, the shallow states might start dispersing in k_x , causing them to become smeared out in the ARPES measurements, possibly beyond our detection limit.

Our model does not take intra-unit-cell potential variations into account, thought to be important for the relatively local Ti $3d$ states. Nonetheless, it is in good qualitative agreement with density-functional theory calculations for the LaAlO₃/SrTiO₃ interface²², which report a similar reconstruction of the electronic structure in the 2DEG into a ladder of sub-bands. The lowest of these was identified as an in-plane Ti d_{xy} state largely localized on the interfacial TiO₂ layer, whereas the charge density from a series of higher-lying d_{xy} states appeared spread out over several layers in the calculation. In addition, these authors found d_{yz} - and d_{xz} -derived states with strongly elliptical Fermi surfaces and high effective masses for transport along x and y , respectively. In the present case, we observe only two concentric isotropic Fermi surfaces of light carriers, which we attribute to the lowest members of a ladder of d_{xy} states. However, we cannot rule out the additional presence of heavy $d_{xz/yz}$ bands in the surface 2DEG, because their intensity would be suppressed relative to d_{xy} states in the experimental geometry and polarization employed here. In addition, the Fermi level in our experiment lies closer to the lowest sub-band minimum than in density functional theory calculations²² for the LaAlO₃/SrTiO₃ interface, and so the $d_{xz/yz}$ states, if present,

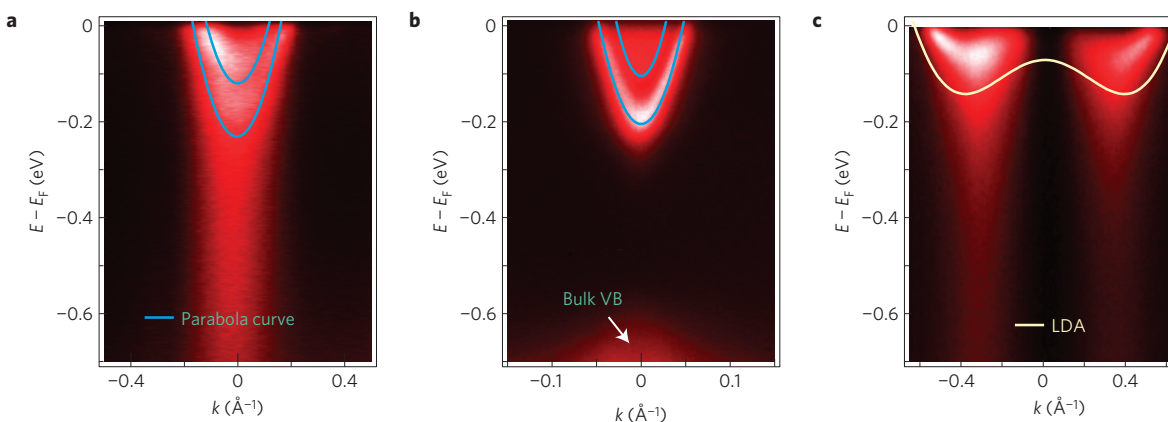


Figure 4 | Comparison of ARPES data from SrTiO₃, InAs and Bi₂Sr₂CuO₆ samples. a, b, 2DEG states at the surface of SrTiO₃ (a) and InAs (b). **c**, ARPES data from the single-layer cuprate Bi₂Sr₂CuO₆ (Bi2201) along $(\pi, 0)$ to $(0, \pi)$. The lines in **a** and **b** are parabolic dispersion relations, to guide the eye, and the result of a local density approximation band-structure calculation in **c**.

should be quite shallow and hence extend deep in the bulk, which would reduce their intensity in ARPES.

Although most conventional semiconductors exhibit a depletion of charge carriers at the surface, a small number have themselves been observed to support a surface 2DEG, concomitant with a downward band bending (ref. 23 and references therein). Comparing the 2DEG states from one such example, InAs (ref. 24) shown in Fig. 4b, with those of SrTiO₃ observed here (Fig. 4a), reveals a qualitative similarity between the two materials. This further confirms the validity of the above model. However, some important differences are also apparent. In particular, there is pronounced spectral weight in SrTiO₃ at binding energies much higher than the band bottom. This effect is absent for the semiconductor case, but can be seen in ARPES measurements of other strongly correlated compounds such as the cuprate high-temperature superconductor Bi₂Sr₂CuO₆ (Fig. 4c; ref. 25). The non-vanishing spectral weight in SrTiO₃ implies a finite electron self-energy at high binding energies, giving direct evidence of enhanced many-body interactions inherent to the 2DEG states of SrTiO₃. Hence, the 2DEG here is best described as an electron liquid rather than an electron gas²⁶. Besides this spectral weight below the band bottom, we also note that the SrTiO₃ data show weak dispersion anomalies (kinks) at a binding energy around 20–30 meV and, less clearly, around 70–80 meV below the Fermi level, which we assign to electron–phonon interactions with a weaker coupling strength than observed in the bulk¹⁴.

In systems where electronic correlations play an important role, the quasiparticles are normally found to be heavy. Intriguingly, however, the strong electron correlations we observe here do not lead to a substantial mass enhancement within the 2DEG. In fact, the effective mass of 0.5–0.6 m_e extracted from the data is lower than the lightest bulk band mass of $\sim m_e$ estimated from ref. 14. Almost certainly, this will apply to the LaAlO₃/SrTiO₃ interface 2DEG too, which helps to explain the high electron mobilities achieved in this system. Although a direct spectroscopic measurement of the electronic band dispersion within the 2DEG, as carried out here, has not yet been achieved in the interface systems, this conclusion is supported by very recent measurements of the penetration field in front-gated LaAlO₃/SrTiO₃ heterostructures, where a 2DEG band mass significantly below any of the bulk masses was inferred²⁷. We speculate that this unusual behaviour might be due to an interaction-induced shrinkage of the fundamental bandgap approaching the surface of SrTiO₃ (ref. 24). This would effectively increase the depth of the potential well and hence result in steeper quantized bands/lighter band masses. If this picture is true, the surface of SrTiO₃, or indeed its interface with LaAlO₃, is a rare

example where many-body interactions have the counter-intuitive effect of increasing the mobility. A full understanding of this will require further theoretical and experimental studies. Spectroscopic investigations of surface 2DEGs, of the form reported here, will probably prove essential to elucidate the fundamental electronic structure and underlying role of many-body interactions in oxide 2DEGs, and so will play a major role in the development of all-oxide electronics.

Received 15 June 2010; accepted 10 December 2010;
published online 16 January 2011

References

- Bednorz, J. G. & Müller, K. A. Perovskite-type oxides: The new approach to high-Tc superconductivity. *Rev. Mod. Phys.* **60**, 585–600 (1988).
- Von Helmolt, R. *et al.* Giant negative magnetoresistance in perovskitelike La_{2/3}Ba_{1/3}MnO_x ferromagnetic films. *Phys. Rev. Lett.* **71**, 2331–2333 (1993).
- Kimura, T. *et al.* Magnetic control of ferroelectric polarization. *Nature* **426**, 55–58 (2003).
- Ohtomo, A. & Hwang, H. Y. A high-mobility electron gas at the LaAlO₃/SrTiO₃ heterointerface. *Nature* **427**, 423–426 (2004).
- Takagi, H. & Hwang, H. Y. An emergent change of phase for electronics. *Science* **327**, 1601–1602 (2010).
- Thiel, S. *et al.* Tunable quasi-two-dimensional electron gases in oxide heterostructures. *Science* **313**, 1942–1945 (2006).
- Reyren, N. *et al.* Superconducting interfaces between insulating oxides. *Science* **317**, 1196–1199 (2007).
- Brinkman, A. *et al.* Magnetic effects at the interface between non-magnetic oxides. *Nature Mater.* **6**, 493–496 (2007).
- Cen, C. *et al.* Nanoscale control of an interfacial metal–insulator transition at room temperature. *Nature Mater.* **7**, 298–302 (2008).
- Mannhart, J. & Scholm, D. G. Oxide interfaces—an opportunity for electronics. *Science* **327**, 1607–1611 (2010).
- Siemons, W. *et al.* Origin of charge density at LaAlO₃ on SrTiO₃ heterointerfaces: Possibility of intrinsic doping. *Phys. Rev. Lett.* **98**, 196802 (2007).
- Kalabukhov, A. *et al.* Effect of oxygen vacancies in the SrTiO₃ substrate on the electrical properties of the LaAlO₃/SrTiO₃ interface. *Phys. Rev. B* **75**, 121404(R) (2007).
- Nakagawa, N., Hwang, H. Y. & Müller, D. A. Why some interfaces cannot be sharp. *Nature Mater.* **5**, 204–209 (2006).
- Meevasana, W. *et al.* Strong energy–momentum dispersion of phonon-dressed carriers in the lightly doped band insulator SrTiO₃. *New J. Phys.* **12**, 023004 (2010).
- Kozuka, Y. *et al.* Optically tuned dimensionality crossover in photocarrier-doped SrTiO₃: Onset of weak localization. *Phys. Rev. B* **76**, 085129 (2007).
- Mochizuki, S. *et al.* Photoluminescence and reversible photo-induced spectral change of SrTiO₃. *J. Phys. Condens. Matter* **17**, 923–948 (2005).
- Aiura, Y. *et al.* Photoemission study of the metallic state of lightly electron-doped SrTiO₃. *Surf. Sci.* **515**, 61–74 (2002).
- Cavaglia, A. D. *et al.* Electric field control of the LaAlO₃/SrTiO₃ interface ground state. *Nature* **456**, 624–627 (2008).

19. Xie, Y. *et al.* Charge writing at the LaAlO₃/SrTiO₃ surface. *Nano Lett.* **10**, 2588–2591 (2010).
20. King, P. D. C., Veal, T. D. & McConville, C. F. Non-parabolic coupled Poisson–Schrodinger solutions for quantized electron accumulation layers: Band bending, charge profile, and subbands at InN surfaces. *Phys. Rev. B* **77**, 125305 (2008).
21. Copie, O. *et al.* Towards two-dimensional metallic behavior at LaAlO₃/SrTiO₃ interfaces. *Phys. Rev. Lett.* **102**, 216804 (2009).
22. Popović, Z. S., Satpathy, S. & Martin, R. M. Origin of the two-dimensional electron gas carrier density at the LaAlO₃ or SrTiO₃ interface. *Phys. Rev. Lett.* **101**, 256801 (2008).
23. King, P. D. C. *et al.* Surface electron accumulation and the charge neutrality level in In₂O₃. *Phys. Rev. Lett.* **101**, 116808 (2008).
24. King, P. D. C. *et al.* Surface band gap narrowing in quantized electron accumulation layers. *Phys. Rev. Lett.* **104**, 256803 (2010).
25. Meevasana, W. *et al.* Hierarchy of multiple many-body interaction scales in high-temperature superconductors. *Phys. Rev. B* **75**, 174506 (2007).
26. Breitschaft, M. *et al.* Two-dimensional electron liquid state at LaAlO₃–SrTiO₃ interfaces. *Phys. Rev. B* **81**, 153414 (2010).
27. Li, L. *et al.* Large capacitance enhancement and negative compressibility of two-dimensional electronic systems at LaAlO₃/SrTiO₃ interfaces. Preprint at <http://arxiv.org/pdf/1006.2847> (2010).
28. Colakerol, L. *et al.* Quantized electron accumulation states in indium nitride studied by angle-resolved photoemission spectroscopy. *Phys. Rev. Lett.* **97**, 237601 (2006).

Acknowledgements

We would like to thank H. Y. Hwang, H. Takagi, M. R. Beasley, J. L. M. van Mechelen, D. van der Marel, P. Reunchan and S. Limpijumnong for helpful discussions. W.M. would like to thank H. Nakajima and Y. Rattanachai for help with the resistivity measurement. The work at ALS and Stanford Institute for Materials and Energy Sciences is supported by DOE's Office of Basic Energy Sciences under Contracts No. DE-AC02-76SF00515 and DE-AC03-76SF00098. The work at St. Andrews is supported by the UK-EPSC (EP/F006640/1) and the ERC (207901). W.M. acknowledges The Thailand Research Fund, Office of the Higher Education Commission and Suranaree University of Technology for financial support.

Author contributions

ARPES measurements were carried out by W.M., P.D.C.K., R.H.H., F.B. and A.T. W.M. and P.D.C.K. analysed the ARPES data. W.M., P.D.C.K. and F.B. wrote the paper with suggestions and comments by R.H.H., S-K.M. and Z-X.S. Calculations of quantized 2DEG states were done by P.D.C.K. S-K.M. and M.H. maintained the ARPES endstation. Resistivity measurements were carried out by W.M. and P.S. Z-X.S. and F.B. are responsible for project direction, planning and infrastructure.

Additional information

The authors declare no competing financial interests. Supplementary information accompanies this paper on www.nature.com/naturematerials. Reprints and permissions information is available online at <http://npg.nature.com/reprintsandpermissions>. Correspondence and requests for materials should be addressed to Z-X.S.

CREATION AND CONTROL OF A TWO-DIMENSIONAL
ELECTRON LIQUID AT THE BARE SrTiO₃ SURFACE

W. Meevasana, P.D.C. King, R.H. He, S.-K. Mo, M. Hashimoto,
A. Tamai, P. Songsirithigul, F. Baumberger, and Z.-X. Shen
(Dated: December 20, 2010)

I. MATERIALS AND METHODS

The measured single crystals are La_xSr_{1-x}TiO₃ (Crystal Base Co., Japan) with $x = 0.001$. The samples are gray in color and partially transparent, confirming their low doping. ARPES data were collected on a Scienta-R4000 analyzer at the Advanced Light Source (ALS), Beamline 10.0.1, with photon energies between 45 - 60 eV and a base pressure of $< 4 \times 10^{-11}$ torr. Additional data, including the valence band spectra shown in Fig. S3, was collected at the Surface and Interface Spectroscopy (SIS) beamline of the Swiss Light Source. All ARPES data was measured with an energy resolution of 6 - 35 meV and an angular resolution of 0.35°. Samples were cleaved at the measurement temperature of $T = 20$ K along notches defining a (100) plane. This results in flatter surfaces than fracturing or scraping of SrTiO₃ as performed previously [1]. Note, however, that the cleaved (100) surface consists of SrO and TiO₂ facets. A recent STM study reports flat terraces of TiO₂ separated by stepped SrO terminations [2]. The typical morphology of the latter renders it unlikely that the well defined 2DEG states observed here are supported by the SrO terminated surface. Hence, we expect that our ARPES data mostly represent the TiO₂ surface. A similar assignment was suggested earlier by Airua et al. [1].

The intensity I of the UV radiation is estimated from the measured photocurrent I_p from the sample and the exposed area of 150 μm (horizontal) times 60 - 100 μm (vertical, depending on beamline settings). The clear (1 \times 1) low-energy-electron-diffraction (LEED) patterns shown in Fig. S1, which were taken after the ARPES measurements, indicate a well-ordered surface devoid of any reconstructions.

To probe the influence of the surface 2DEG formation on the transport properties of SrTiO₃, we also measured the resistivity at the surface of undoped SrTiO₃ both before and after UV irradiation. The measurements were performed at room temperature in vacuum (pressure $< 1 \times 10^{-8}$ mbar, on Beamline 3.2a of the Synchrotron Light Research Institute (SLRI), Thailand) using a Keithley electrometer. After irradiation with similar doses as in the ARPES work we observed a drop in resistivity by a factor of ≈ 20 , consistent with the formation of a conducting 2DEG.

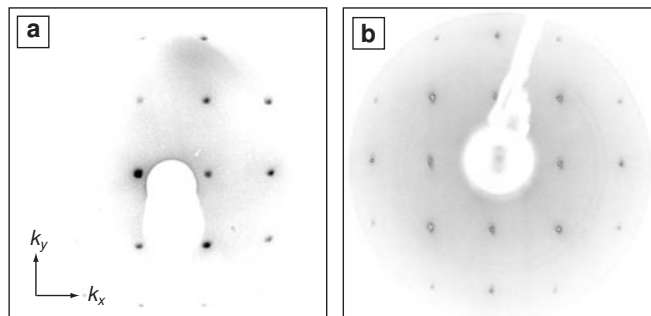


FIG. S1: Low energy electron diffraction (LEED) patterns of La_xSr_{1-x}TiO₃ showing clear c(1x1) patterns with no sign of surface reconstruction. a) LEED pattern from a $x = 0.001$ sample, taken at $T = 20$ K immediately after the ARPES measurements. b) A similar diffraction pattern is observed in a $x = 0.05$ sample with much higher carrier density.

A. 2D character of the observed bands

We confirmed the absence of significant band dispersion along the direction perpendicular to the surface (k_z) by varying the incident photon energy. Fig. S2a-e show dispersion plots of the 2DEG states for photon energies ranging from 45 eV to 65 eV corresponding to estimated k_z values of 2.6 - 3.8 π/a . The Fermi momenta k_F extracted from this data (Fig. S2f) are constant within our experimental accuracy, indicating a highly two-dimensional (2D) character of the observed bands. The in-plane parabolic $E(k)$ dispersion relation with no dispersion along k_z , as directly measured here, is the defining property of a 2DEG.

B. Changes in the valence band spectra with UV light exposure

We have shown in the main text that the surface charge density can be modified by increasing the irradiation dose to which the surface is exposed. Here, we discuss the corresponding changes in the oxygen valence band in more detail.

Fig. S3 shows angle-integrated photoemission (AIPES) valence band spectra for different exposures to dim UV light ($I_p = 0.38$ nA). At $t = 0$ (black line), the spectrum shows clear oxygen 2p (O2p) states between $\sim 3 - 9$ eV, and no significant spectral weight in the band gap (0 - 3 eV). As the exposure time increases, the spectral weight of the O2p state decreases slightly and its

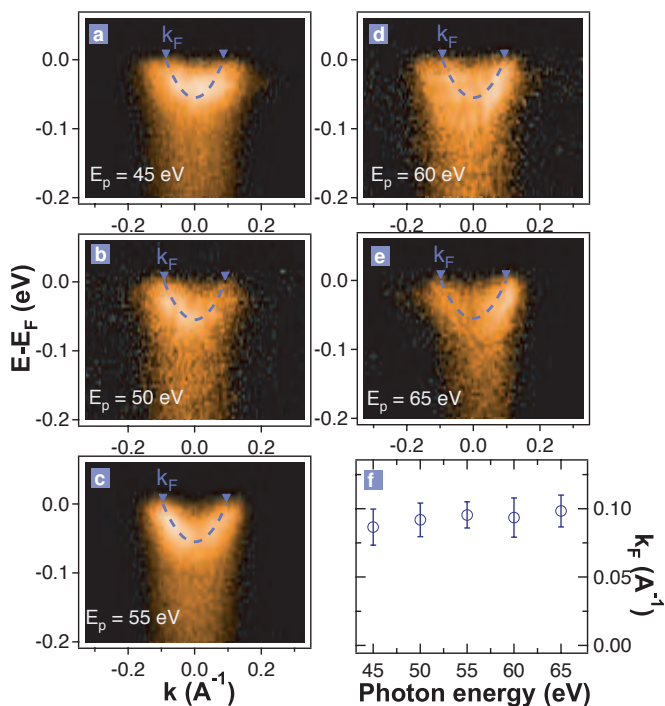


FIG. S2: Photon energy dependence of ARPES data indicating negligible k_z dispersion. a)-e) show ARPES data measured with low photon flux at various photon energies E_p indicated in the figure. The sample has been exposed to $\sim 60 \text{ J/cm}^2$ prior to the first measurements shown in panel a). f) summarizes the Fermi momenta k_F extracted from a)-e). The range of photon energies corresponds to estimated k_z values from $2.6 - 3.8\pi/a$.

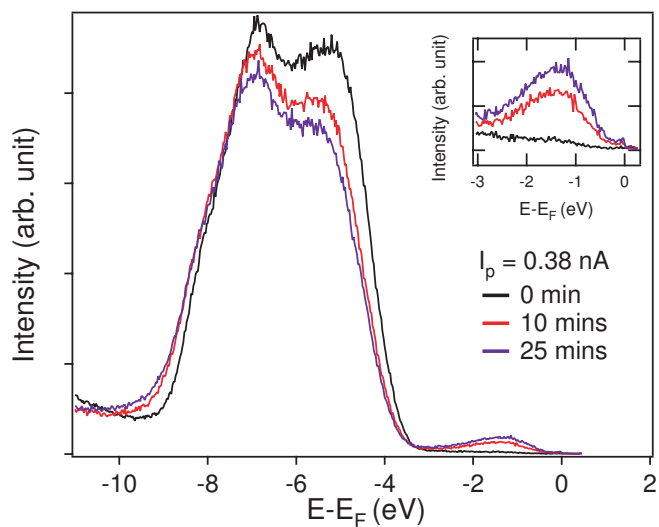


FIG. S3: Evolution of the valence band (VB) spectra of SrTiO_3 from the pristine cleaved surface to the exposed surface. The inset shows the evolution of the in-gap state with increasing exposure to UV light.

leading edge shifts to higher binding energy. This indicates an increase in the valence band maximum to surface Fermi level separation, consistent with a downward band bending and development of a 2DEG at the surface, as discussed in the main text. We note that a recent study on semiconductor surface 2DEGs [3] indicates that the valence and conduction band bendings do not need to be equal, due to many-body interactions within the surface 2DEG. Indeed, the valence band bending puts a lower limit on the amount of downward bending of the conduction band, consistent with the situation we observe here.

Together with the valence band shift we also observe a broad in-gap state developing at a binding energy of $\sim 1.3 \text{ eV}$. Following earlier studies, we consider that this state is most likely associated with oxygen vacancies at the surface [1], which we attribute as the origin of the donor defect states inducing the 2DEG which we observe following UV-irradiation.

We also note, however, that hydrogen can act as a donor in perovskite titanate compounds [4, 5], providing a second possible source of the microscopic donor surface states. We experimentally confirmed that exposure to the residual gases from the vacuum alone was not sufficient to induce the 2DEG states by performing AIPES measurements at different positions on the same sample. Since the light spot size is much smaller than the sample this allows us to separate the influence of residual gas and exposure to UV light. Moving to a previously unexposed area after performing the measurements described above, we find that the valence band fully recovers to the $t = 0$ spectrum from Fig. S3. Only following sufficient UV light exposure, the in-gap state develops again and the valence band shifts to higher binding energy. This confirms that UV light exposure is crucial for the development of the 2DEG states. However, as SrTiO_3 is known to promote photocatalysis [6], we cannot exclude that, in the presence of residual water vapor in the vacuum, the exposure to UV light could generate atomic hydrogen at the surface. Hydrogen adsorption at the surface could also give rise to the in-gap defect peak that we observe [4], and we cannot distinguish between this and oxygen vacancies with our experimental measurements. This should therefore be the subject of future investigations. However, our analysis and conclusions presented in the main manuscript are not sensitive to the exact microscopic nature of the defects causing the charge accumulation.

C. Calculations

The downward bending of the conduction band and dispersions of the 2DEG states are described by a non-parabolic coupled Poisson-Schrödinger scheme, described in detail elsewhere [7]. In the calculations, the downward conduction-band bending is -0.7 eV at the surface, the bulk band gap is 3.3 eV , the bulk electron concentration is $1.8 \times 10^{19} \text{ cm}^{-3}$ and the effective mass is set to

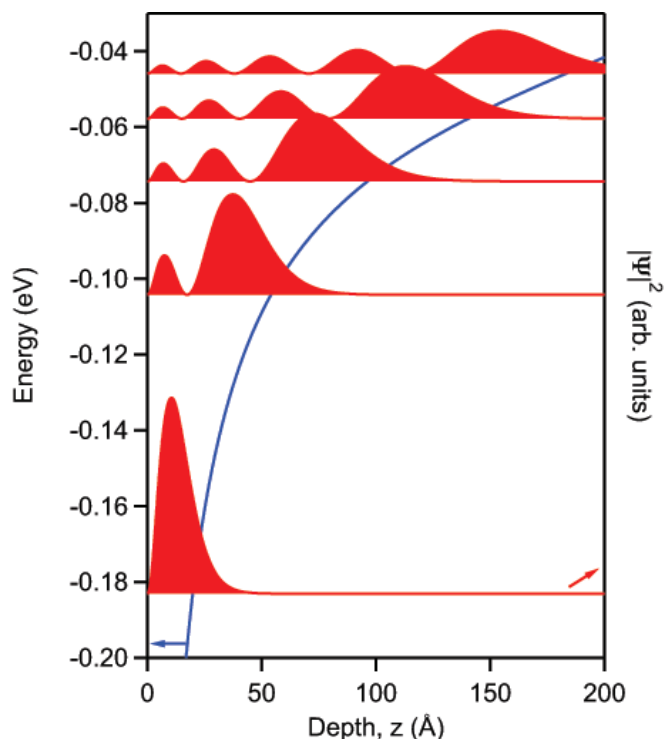


FIG. S4: Poisson-Schrödinger calculations of the surface-normal component of the eigen-functions (red) of the quantized states within the potential well caused by the downward band bending (blue). The modulus squared of the eigen-functions are shown, vertically offset to the respective subband binding energy within the well.

$0.6m_e$. The bulk dielectric constant is set to 8000 at $T=20\text{K}$ and zero-field and an electric-field dependent susceptibility model [8] is incorporated. An iterative approach is used to ensure self-consistency between the dielectric constant and band bending potential variation as a function of depth below the surface.

The result of realistic calculations is shown in Fig. 3 of the main manuscript. We find a rapid downward band bending, causing the conduction-band states to become quantized into a ladder of subbands. The surface-normal component of their wave functions are shown in Fig. S4. The wave function of the lowest subband is peaked less than 3 unit cells from the surface, while the probability density of the higher-lying subbands progressively extend deeper in the bulk. Together, these lead to an increase in charge density, strongly peaked in a narrow region ($\sim 10\text{Å}$) close to the surface. This narrow spatial extent of the increased charge density, resulting from the strongly confined nature of particularly the lowest subband wave function, strongly supports the two-dimensional character of the 2DEG states observed from ARPES.

To further verify such a strongly confined nature of the observed electronic states, we have performed additional calculations where we artificially force the band bending to occur over larger distances. Consequently, the increased electron density approaching the surface is

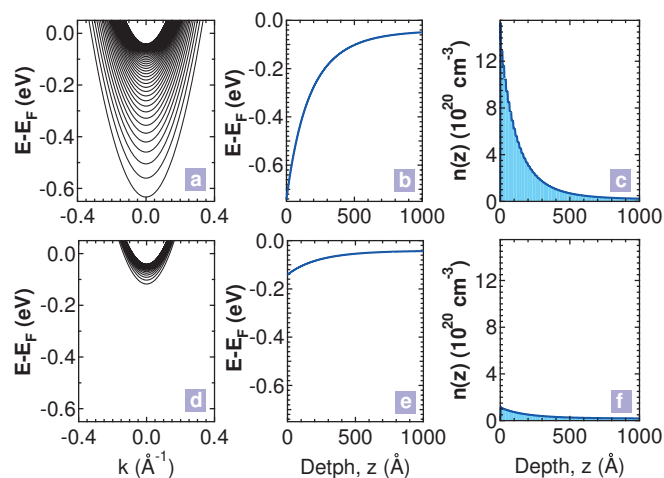


FIG. S5: Calculations of quantized states with the increased charge density wide-spread in sample depth. Both calculations are performed with a more three-dimensional (3D) character of the charge density increase in the vicinity of the surface, with the depth characterizing the band bending increased by a factor of approximately 10 relative to the calculation shown in Fig. 3 of the main manuscript. In (a)-(c), the conduction band bending is set to -0.7eV at the surface, as in Fig. 3, while in (d)-(f), the conduction band bending is set to -0.1eV . The calculations yield many quantized states as shown in (a) and (d). The band bendings as a function of sample depth are shown in (b) and (e), while the corresponding 3D charge density variations are shown in (c) and (f).

spread further into the bulk (that is, the system becomes more three-dimensional), as shown in Fig. S5. For the calculation in Fig. S5a-c, the conduction-band bending is kept at -0.7eV (as in Fig. 3 of the main manuscript) but the effective width is extended by a factor of approximately 10. The electronic states in such a situation rapidly approach a continuum limit, resulting in many subbands and a large sheet density of $1.9 \times 10^{15}\text{cm}^{-2}$ which is much higher than the value extracted from the ARPES data. An order-of-magnitude lower sheet density, much closer to the experimentally-observed value, can be obtained by reducing the magnitude of the band bending to 0.1eV , as shown in Fig. S5d-f. However, the resulting calculations still show large discrepancies with the measured ARPES: the calculated 2DEG states are shallower than the measured states by approximately a factor of two, while there are still many more subbands predicted than are observed. Further, this degree of band bending is unreasonably small, being smaller than the shift of the valence band seen in Fig. S3 which puts a lower limit on the amount of conduction band bending. These calculations, therefore, confirm that a more three-dimensional character of the electron gas formed at the surface of SrTiO_3 following UV-irradiation than considered in the main manuscript is inconsistent with the electronic states that we directly observe from ARPES, thus further validating their two-dimensional nature.

-
- [1] Aiura, Y. *et al.* Photoemission study of the metallic state of lightly electron-doped SrTiO₃. *Surf. Sci.* **515**, 61 (2002), *and references therein*.
- [2] Guisinger, N. P. *et al.* Nanometer-Scale Striped Surface Terminations on Fractured SrTiO₃ Surfaces. *ACS Nano.* **3**, 4132 (2009).
- [3] King, P. D. C. *et al.* Surface band gap narrowing in quantized electron accumulation layers. *Phys. Rev. Lett.* **104**, 256803 (2010).
- [4] Lin, F. *et al.* Hydrogen-induced metallicity of SrTiO₃ (001) surfaces: A density functional theory study *Phys. Rev. B* **79**, 035311 (2009), *and references therein*.
- [5] Xiong, K., Robertson, J. & Clark, S. J. Behavior of hydrogen in wide band gap oxides. *J. Appl. Phys.* **102**, 083710 (2007).
- [6] Miyauchi, M., Takashio, M., & Tobimatsu, H. Photocatalytic Activity of SrTiO₃ Codoped with Nitrogen and Lanthanum under Visible Light Illumination *Langmuir* **20**, 232-236 (2004).
- [7] King, P. D. C., Veal, T. D. & McConville, C. F. Non-parabolic coupled Poisson-Schrodinger solutions for quantized electron accumulation layers: Band bending, charge profile, and subbands at InN surfaces. *Phys. Rev. B* **77**, 125305 (2008).
- [8] Copie, O. *et al.* Towards Two-Dimensional Metallic Behavior at LaAlO₃/SrTiO₃ Interfaces. *Phys. Rev. Lett.* **102**, 216804 (2009).